JOURNAL OF PROPULSION AND POWER
Vol. 18, No. 2, March–April 2002

Rotor Blade-to-Blade Wake Variability and Effect on Downstream Vane Response

Albert J. Sanders* and Sanford Fleeter†
Purdue University, West Lafayette, Indiana 47907

Experiments are performed in a high-speed fan stage to investigate multistage interaction effects on rotor blade-to-blade wake variability and the resulting downstream vane row unsteady aerodynamic response. Multistage effects on the rotor wake are quantified by acquiring data encompassing two complete rotor revolutions at each of several inlet guide vanes clocking positions relative to downstream stationary probes. The resulting downstream vane response data are acquired over a range of steady loading conditions, with both design and off-design operation of the rotor considered. Multistage interactions significantly affect the rotor wake characteristics and lead to the possible generation of rogue wakes. The fundamental periodicity of these interactions is one complete rotor revolution due to the unequal number of blades and vanes in the machine. The rotor wake and resultant vane row unsteady aerodynamic response variability are also quantified. Off-design rotor operation results in wakes with the largest variability, that is, on the order of the average velocity deficit. The variability of the vane response is even more pronounced, as large as 160% of the maximum average unsteady lift over one blade pass period.

Nomenclature

C	=	stator vane chord
C_L	=	unsteady lift coefficient
C_M	=	unsteady moment coefficient
C_p	=	pressure coefficient
N_c	=	corrected rotor speed
p	=	static pressure
S_{igv}	=	inlet guide vanes (IGV) tangential spacing
T_{BP}	=	blade pass period
t	=	time
V	=	absolute velocity magnitude
α	=	absolute flow angle (cw)
Δp	=	airfoil unsteady pressure difference, $p_{\text{ps}} - p_{\text{ss}}$
ΔS	=	IGV clocking position
θ_{igv}	=	IGV stagger angle
ρ	=	density
σ	=	standard deviation

Subscripts

av	=	time-average value
ps	=	airfoil pressure surface
ss	=	airfoil suction surface
·	=	freestream value

Introduction

BLADE row interactions in turbomachines are an important concern in the design and development of advanced gas turbine engines, with wakes shed by upstream airfoil rows being the most common source of unsteady aerodynamic excitation. However, actual turbomachine wakes always exhibit some blade-to-blade variability due to sources such as airfoil manufacturing differences, as well as their having aerodynamic origins.

In multistage turbomachines, downstream blade rows periodically chop upstream-generated wakes, with the wake segments reoriented as they are transported though the rotor passage. In compressors, these chopped wake segments do not become reunited at the rotor exit due to the blade circulation and thereby cause attenuation of the wake segments by dispersion.[1] This attenuation occurs because the chopped wake segments gain more stagnation enthalpy than the freestream flow as they pass through the rotor. Circumferential nonuniformities in the exit total temperature have also been attributed to the passage of rotor wakes through a downstream stator row.[2] This is due to rotor wake rectification resulting from the transport of the wake segments relative to the mean flow as they pass through the stator, with the wakes collecting on the stator pressure surfaces.

The interaction effects were quantified by circumferentially traversing a hot wire behind each blade row of a low-speed compressor.[3] Both the depth and width of the rotor wakes increased when the rotor trailing edge was within the stationary inlet guide vane (IGV) wake street. Sharma et al.[4] found that the rotor exit flow from a $1\frac{1}{2}$-stage low-speed turbine exhibited a strong dependence on the circumferential location of the rotor airfoils relative to the upstream vanes, with both maximum and minimum interaction times identified. Johnston and Fleeter[5] circumferentially indexed the IGV row of a single-stage high-speed fan relative to stationary instrumentation. At certain indexing positions, the chopped IGV wake segments could be either in- or out-of-phase with the rotor wakes, with the in-phase position resulting in deeper rotor wakes.

For embedded airfoil rows, both stator–stator and rotor–rotor interactions are also possible. A cyclic waxing and waning of the unsteadiness around the annulus of a high-speed compressor due to the interaction between the wakes of first- and second-stage rotor airfoils was found, with some of the first-stage rotor wakes passing through the second-stage rotor passages uninterrupted whereas other wakes impinged on the second-stage rotor blades themselves.[6] Turbomachine stages generally feature unequal numbers of rotors and stators. Thus, at any instant in time, these multistage interactions vary around the annulus, with some rotor wakes interacting with adjacent airfoil rows while others do not. Note that the spatial periodicity of these interactions is, thus, over the entire annulus.

High cycle fatigue (HCF) caused by flow-induced vibrations is a universal problem in the gas turbine industry. In fact, the loss of blades or disks due to HCF is currently the predominant surprise engine failure mode in the field. The inability to predict or

Received 10 October 2000; revision received 16 June 2001; accepted for publication 25 June 2001.

*Research Assistant, School of Mechanical Engineering, 1288 Mechanical Engineering.

†McAllister Distinguished Professor, School of Mechanical Engineering, 1288 Mechanical Engineering. Fellow AIAA.

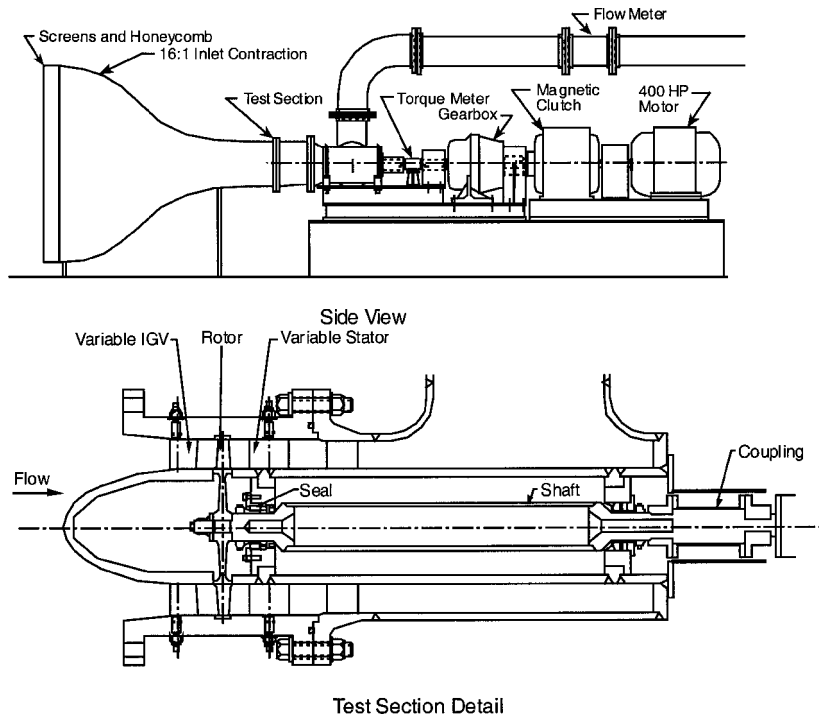

Fig. 1 Purdue High-Speed Research Axial Fan.

understand these failures may be due to variability. Structural and material property variabilitiesare being addressed.However, a probabilistic approach has not been utilized with regard to the unsteady aerodynamics.

This paper addresses these multistaging and variability effects on HCF unsteady aerodynamics. Specifically, the effects of multistage unsteady aerodynamic interactions on rotor blade-to-blade wake variability and the resulting downstream vane row unsteady aerodynamic response are investigated. This is accomplished through experiments performed in the Purdue High Speed Research Axial Fan Facility. Multistaging effects on the rotor-wake-generatedforcing function are quantified by acquiring detailed data encompassing two complete rotor revolutions at each of several IGV clocking positions relative to downstream stationary probes. The resulting downstream vane row unsteady aerodynamic response data are acquired with the IGV in the nominal unclocked position in the same manner. The variabilities of both the rotor wakes and the vane responses over one complete rotor revolution are also quantified.

Research Facility

The Purdue High Speed Research Axial Fan Facility features a $1\frac{1}{2}$-stage configuration consisting of 18 IGVs, a blisk with 19 rotor blades, and 18 stator vanes (Fig. 1). The stage is of a low aspect ratio design with a 0.67 hub–tip ratio and 30.48 cm (12.00 in.) diameter. The IGVs and rotor blades comprise NACA 65 series airfoil profiles on circular arc mean lines, and the stators are of a low-camber controlled-diffusiondesign[7] (Fig. 2). The chord length of the IGV varies from 35.5 mm (1.40 in.) at the root to 53.3 mm (2.10 in.) at the tip, the rotor chord length is 50.8 mm (2.00 in.), and the stator chord length is 76.2 mm (3.00 in.). The IGV–rotor and rotor–stator midspan axial spacings are both 62.4% stator chord (94% rotor chord). The IGV row is indexable, thereby permitting vane row clocking effects to be investigated.

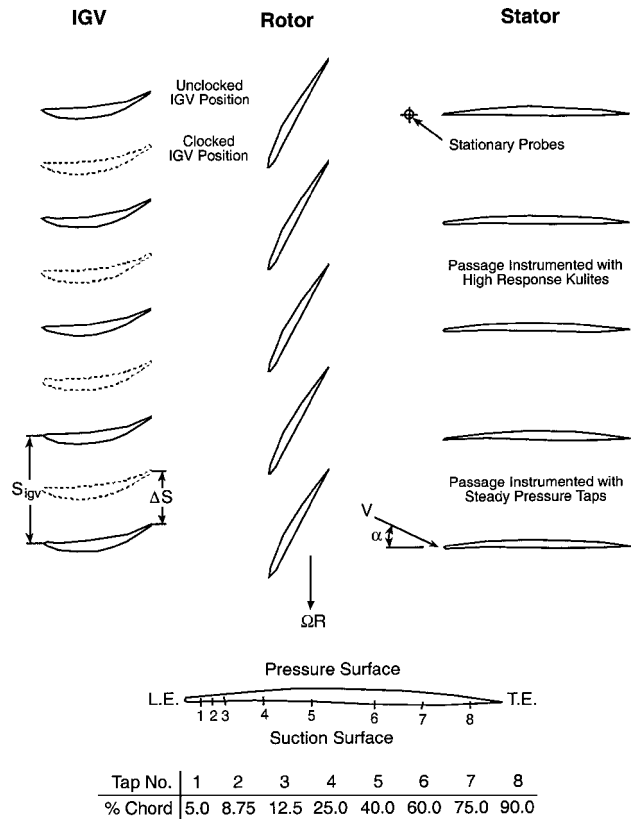

Fig. 2 Stage geometry showing instrumentation locations and vane clocking.

Data Acquisition and Analysis

Phase-lock-averaged measurements of the time-variant rotor wake velocity components and static pressure are measured at midspan along with the downstream stator steady and unsteady surface pressures. A cross hot film and an unsteady static pressure probe measure the rotor wakes. The resulting stator unsteady aerodynamic response is measured with high-response Kulite XCS-093 pressure transducers reverse mounted within the suction surface of one vane and the pressure surface of an adjacent vane (Fig. 2). These transducers are statically calibrated after installation and have a nominal sensitivity of 15 mV/psi (217.4 mV/bar), with frequency responses of 20 and 50 kHz for the instrumented vanes and the static pressure probe. Time-average measurements of the casing static pressure, midspan total pressure, and midspan total temperature are also made at the same axial location as the hot film. To minimize probe interference effects, all instrumentation is located 18.75% stator chord upstream

of the vane leading edge and circumferentially positioned in line with the leading edges of vanes adjacent to the instrumented passages (Fig. 2), which is drawn to scale.

All signals are low-pass filtered at 200 kHz to prevent aliasing, with the signals from the static pressure probe and the instrumented vanes also high-pass filtered at 500 Hz before amplification to remove harmonics of 60-Hz line noise. Phase-lock averaging is used, with the data acquisition triggered by a once-per-revolution pulse from a photooptic sensor mounted on the compressor shaft. For each data ensemble, the time-variant signals are digitized at a rate of 1 MHz, with the number of samples chosen to encompass two complete rotor revolutions. Each of these ensembles is then averaged over 500 revolutions and stored to disk, with the time-variant signals shifted in time before analysis to represent the time-variant flowfield of a single vane.

All pressures are nondimensionalized by the time-average inlet dynamic head,

$$C_p = \frac{p - p_\infty}{1/2\rho_\infty V_{\text{av}}^2} \tag{1}$$

where for the steady pressure, p is the time-average pressure and p. is the time-average pressure measured on the casing wall upstream of the vane leading edge, both measured with pneumatic instrumentation. For the unsteady vane response and static pressure probe data, $p - p$. is the fluctuation in static pressure measured by AC coupling the pressure transducer signals.

The time-variant vane response is described by unsteady lift and moment coefficients, with the integrals evaluated from the leading-edge to the trailing-edge tap locations.

$$C_L = \frac{1}{C}\int_{0.05C}^{0.9C} C_{\Delta p}\,\mathrm{d}x \tag{2a}$$

$$C_M = \frac{1}{C^2}\int_{0.05C}^{0.9C} (x - 0.25C)C_{\Delta p}\,\mathrm{d}x \tag{2b}$$

Results

To investigate rotor blade-to-blade wake variability and the resulting vane row unsteady aerodynamic response, experiments are performed in the Purdue High Speed Research Axial Fan. Two midspan IGV stagger angles are investigated: 20 deg, which results in a nearly axial rotor exit flow, and 10 deg, which results in approximately 10 deg of rotor exit swirl. Additionally, the stators are set at 0-deg stagger, thus, these two IGV staggers result in different stator angles of attack, thereby allowing the effects of steady vane loading to be assessed. At each IGV stagger, data are acquired at corrected speeds of 15,000 and 18,000 rpm. Previous pressure sensitive paint measurements at 10-deg IGV stagger indicate that rotor shock formation occurs near a corrected speed of 16,000 rpm (Ref. 8).

Rotor Wake Multistage Interactions

The rotor wakes are the unsteady aerodynamic forcing function to the downstream stator. However, these wakes are not steady in the rotor relative frame due to the interaction of the rotor with the upstream IGV row and the potential field of the downstream stator row. To quantify these multistage interaction effects on the rotor wake, the IGV row is circumferentially clocked over one vane spacing relative to the stationary instrumentation and downstream stator at a corrected speed of 15,000 rpm. Because the data acquisition is always initiated at the same absolute rotor shaft position, the temporal variations over one complete rotor revolution measured by the stationary probes are generated by the same rotor blades, regardless of IGV clocking position. However, by clocking the IGV row, the interaction between the IGV and the rotor is shifted in the time domain, thereby resulting in different rotor wake characteristics. Thus, multistage interaction effects are assessed by comparing the time-variant signals from the stationary probes at the different IGV clocking positions. In the unclocked position, the stacking axes of the IGV and the stator airfoils coincide at the same circumferential position (Fig. 2).

Figures 3–5 show the rotor exit time-variant midspan velocity, flow angle, and static pressure over one rotor revolution as a function of IGV clocking position for 20-deg IGV stagger. This is the inlet flowfield to the vane row, with the 19 rotor-blade wakes readily apparent. The first blade wake is also shown at the beginning of the second rotor revolution to illustrate that the fundamental temporal periodicity of these multistage interactions is over one complete rotor revolution.

Both the rotor blade wake deficits and the freestream velocities change noticeably as the IGV row is clocked (Fig. 3). This is attributed to multistage interactions, with the chopped IGV wake segments most visible in the freestream region at the one-quarter-cycle IGV position. The wake velocity deficit is similar for the unclocked and one-half-cycle IGV positions, with the wakes for the one-half-cycle position narrower than those in the unclocked position. The wakes for the one-quarter- and three-quarter-cycle IGV positions are also similar, with the velocity deficits approximately 5% smaller than those in the unclocked position. The one-half-cycle IGV data also reveal a very interesting phenomenon. Namely, the magnitudes of the velocity deficits are nearly the same as those in the unclocked position, but the blade-to-blade wake variability is markedly different. In the unclocked position, blade-to-blade variability is apparent. However, in the one-half-cycle IGV position, the wakes are fairly uniform from blade-to-blade except for a rogue wake with a velocity deficit roughly 2.5% larger than the other blades between the 17th and 18th blade pass periods. This rogue wake is also evident in the three-quarter-cycle IGV clocking position and to a lesser extent in the one-quarter-cycle position. Also, the freestream velocity magnitude is similar for the unclocked and the full-cycle IGV positions. However, the waveforms exhibit small differences, with the suction side of the rotor blade wake thicker in the unclocked position. Note that for each clocking position the temporal periodicity is one complete rotor revolution, with the wake generated by the first blade identical for the first and second rotor revolutions.

Figure 4 shows that blade-to-blade wake differences in the absolute flow angle of up to 3 deg exist at each IGV clocking position.

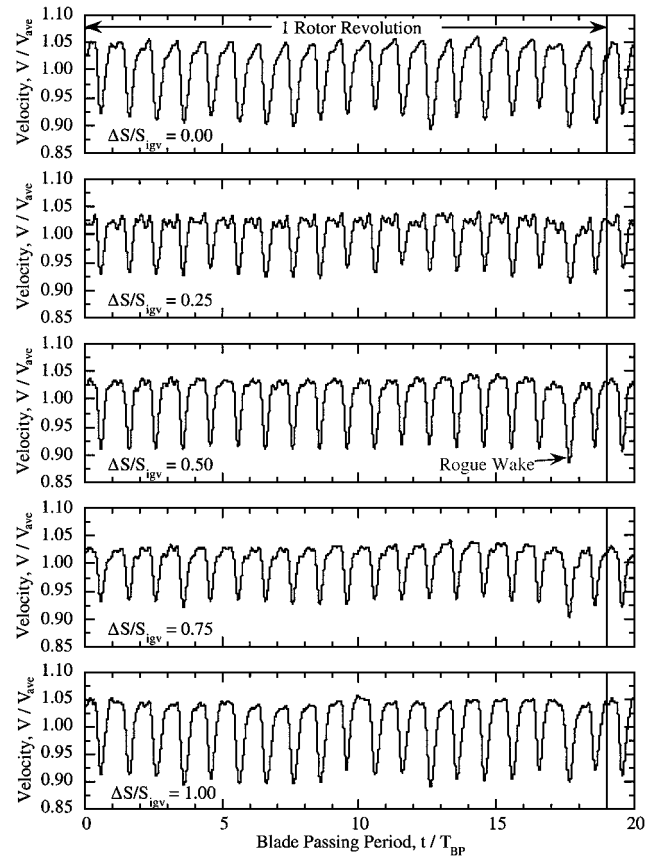

Fig. 3 Velocity magnitude as a function of IGV clocking, $\theta_{\text{igv}} = 20$ deg and $N_c = 15{,}000$ rpm.

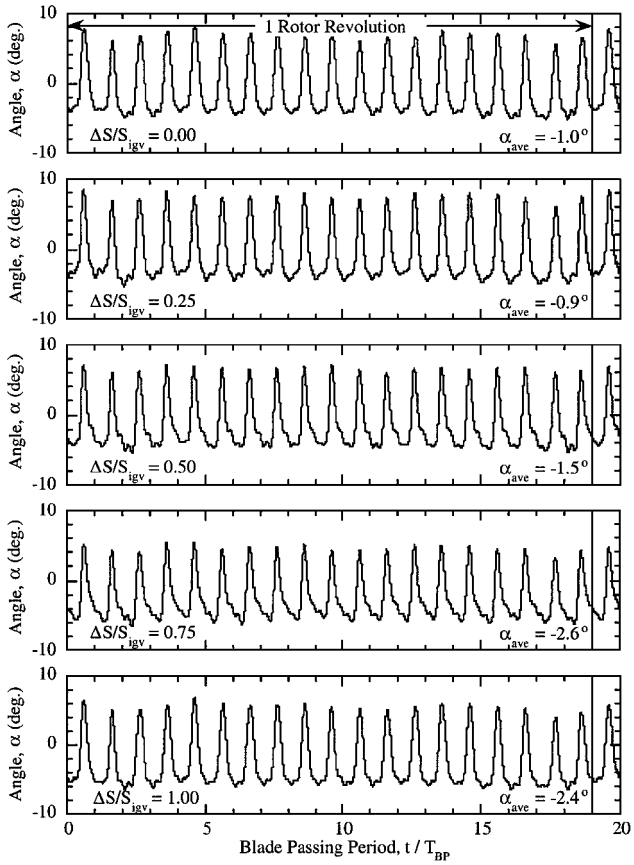

Fig. 4 Flow angle as a function of IGV clocking, $\theta_{igv} = 20$ deg, and $N_c = 15{,}000$ rpm.

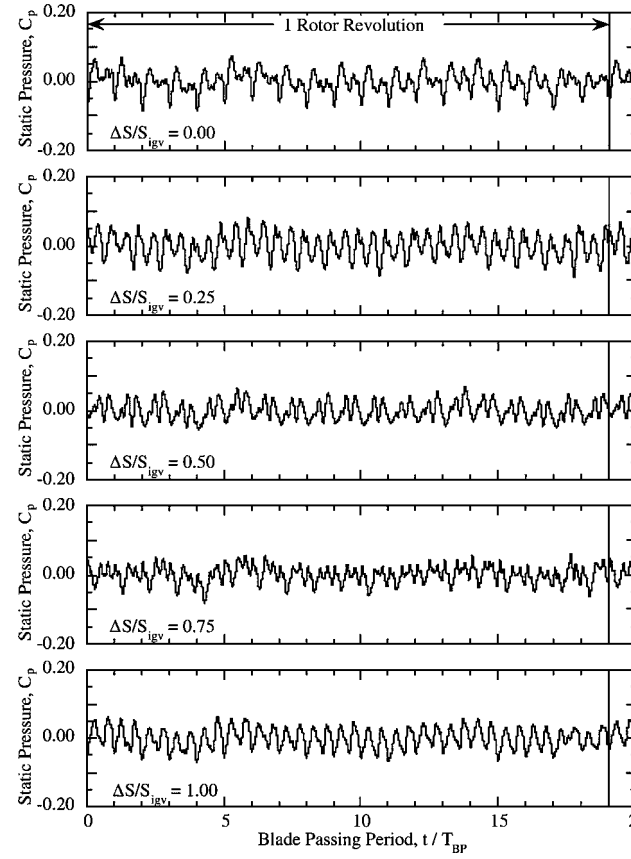

Fig. 5 Static pressure as a function of IGV clocking, $\theta_{igv} = 20$ deg and $N_c = 15{,}000$ rpm.

However, this wake variability as well as the magnitudes of the flow angle variations are very similar for each IGV clocking position, not exhibiting the differences seen in the velocity data. The most notable difference is in the time-average flow angle that varies from −0.9 to −2.6 deg as the IGV is clocked over one cycle. Also, the time-average flow angle is different for the unclocked and full-cycle positions, indicating that the fundamental spatial periodicity is over the entire compressor annulus and not just a single vane spacing.

The static pressure coefficient data of Fig. 5 were acquired 66% rotor chord downstream of the rotor. Hence, the steady rotor potential flowfield is expected to be negligible and not contribute to the unsteady static pressure. However, the data exhibit large pressure perturbations at blade-pass-frequency harmonics. Also, both the waveform character and its phase change with IGV clocking position, with the waveforms for the unclocked and full-cycle IGV positions significantly different.

These pressure perturbations are attributed to acoustic interactions. Rotors and stators interact and generate spinning acoustic modes at multiples of blade-pass frequency. Depending on the axial wave number, these modes either decay exponentially or propagate unattenuated. These interactions lead to frequency shifting and mode scattering, with a single excitation frequency in the rotor frame producing a multiplicity of frequencies and interblade phase angles in the stator frame.[9]

That the static pressure waveforms differ at the unclocked and full-cycle IGV positions supports the hypothesis that these pressure perturbations are due to acoustic interactions, that is, the pressure perturbations due to these spinning acoustic modes vary with circumferential position and depend on the mode order. The clocking of the IGV row results in a shifting of the IGV–rotor interaction in the time domain. Hence, the phases of the acoustic modes generated by this IGV–rotor interaction are also shifted. In addition, the interaction between the rotor and downstream stator generates a second set of acoustic modes, with the phase of these modes independent of IGV clocking position. Because the probe measures the total interaction field, both sets of acoustic interaction modes are contained in the data, with possible constructive or destructive interference between the two sets of modes occurring as the IGV is clocked over one cycle. Thus, this multistage interaction also contributes to the rotor wake differences resulting from IGV clocking.

Figures 6–8 show analogous results for the 10-deg IGV stagger. The rogue wake is more pronounced and clearly evident at all IGV clocking positions, with its velocity deficit nearly twice that of the other wakes in the unclocked position. The freestream region ripples are the chopped IGV wake segments, which are much more pronounced than in Fig. 3. This is due to the IGV incidence increase from −3.4 to −13.4 deg in going from the 20- to the 10-deg IGV stagger resulting in larger IGV wakes. At the three-quarter-cycle IGV position, these chopped IGV wake segments have actually merged with the rotor wakes, resulting in a markedly different wake profile from those at the other clocking positions. Also, the unclocked and full-cycle IGV results are not identical, with the deficits associated with the wakes of the 3rd, 11th, and 14th blades differing. The temporal periodicity at each clocking position is again over one complete rotor revolution, with the spatial periodicity over the entire annulus due to the differences noted for the unclocked and full-cycle IGV positions. The rotor exit absolute flow angle variability is nearly independent of IGV clocking (Fig. 8). However, the flow angle fluctuations are about 1 deg larger for the one-half-cycle vs the other IGV clocking positions. The time-average flow angles for the clocked and full-cycle IGV positions are also identical, in contrast to the 20-deg IGV stagger results.

Figure 8 shows the rotor exit unsteady static pressure coefficient as a function of IGV clocking position. As per the 20-deg IGV stagger, the waveform character and phase change with IGV clocking. However, the waveforms for the unclocked and full-cycle positions are nearly identical and the pressure fluctuations are larger than those at the 20-deg IGV stagger. Also, both the character and phase of the three-quarter- and full-cycle waveforms are similar to the 20-deg IGV stagger unclocked and one-quarter-cycle positions of Fig. 5.

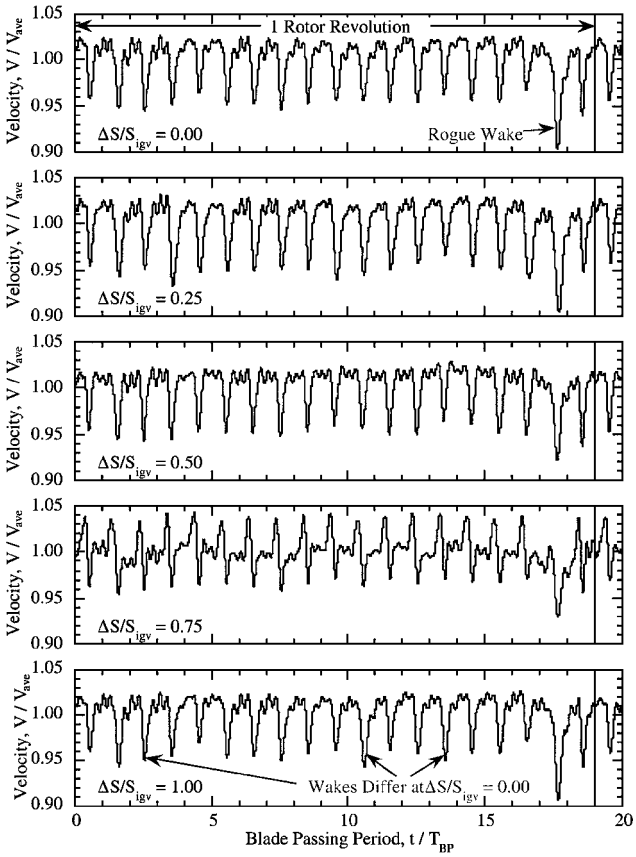

Fig. 6 Velocity magnitude as a function of IGV clocking, $\theta_{igv} = 10$ deg and $N_c = 15{,}000$ rpm.

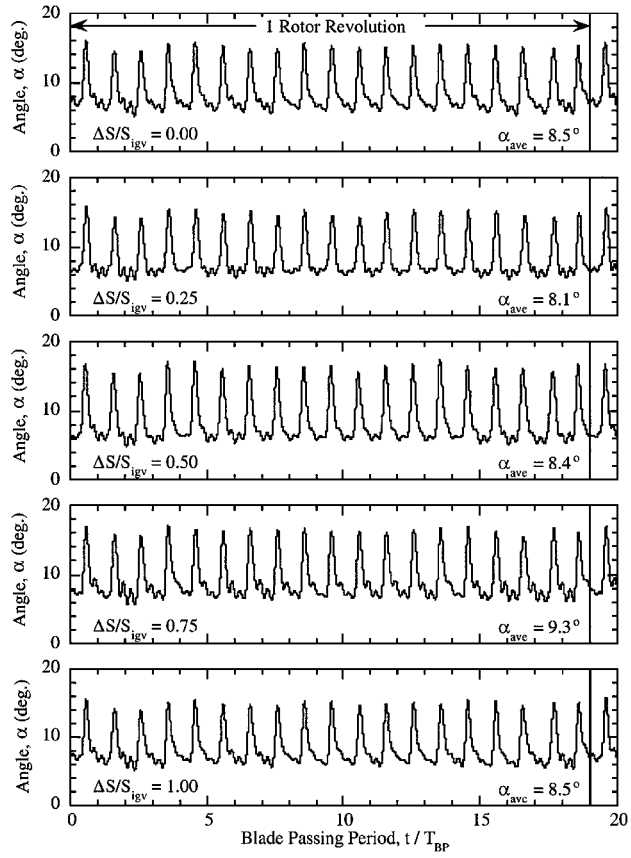

Fig. 7 Flow angle as a function of IGV cocking, $\theta_{igv} = 10$ deg and $N_c = 15{,}000$ rpm.

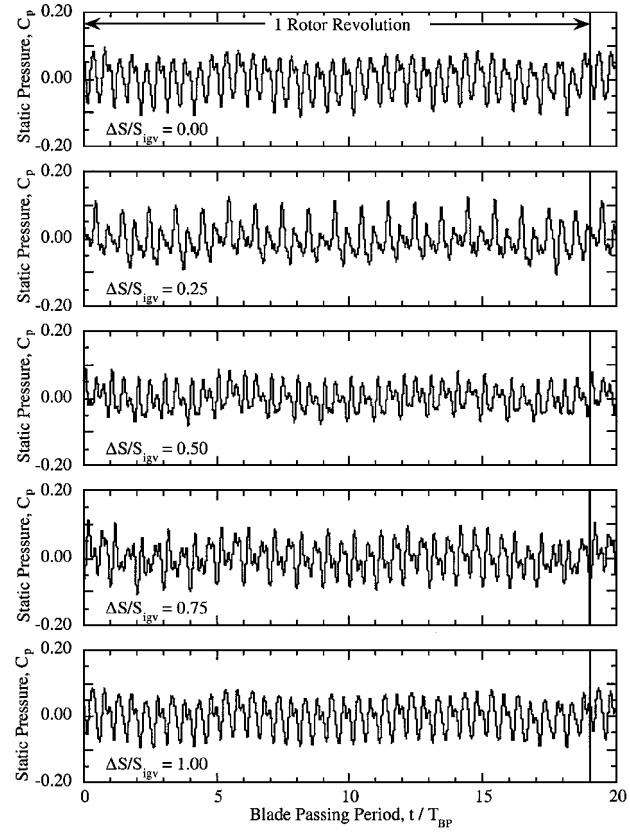

Fig. 8 Static pressure as a function of IGV clocking, $\theta_{igv} = 10$ deg and $N_c = 15{,}000$ rpm.

Vane Unsteady Aerodynamic Response

The unsteady aerodynamic response of the downstream vane row over one complete rotor revolution is also examined. To illustrate the fundamental temporal periodicity, the response data are presented for 20 rotor blade-pass periods. These detailed response data are acquired at corrected speeds of 15,000 and 18,000 rpm for IGV staggers of 10 and 20 deg with the IGV row in the unclocked position. The steady vane pressure distributions are presented in Fig. 9. The pressure distributions for angles of attack of −1.0 and 8.5 deg are in good qualitative agreement with the results obtained in a linear oscillating cascade with the airfoils staggered at 60 deg (Ref. 7).

Figures 10 and 11 show the rotor-wake-generated forcing function and the resultant vane row unsteady aerodynamic response at corrected speeds of 15,000 and 18,000 rpm for the 20-deg IGV stagger. Presented are the rotor wake velocity deficit, flow angle, and static pressure together with the resulting vane unsteady lift and moment, with the two speeds corresponding to design (subsonic) and off-design (transonic) rotor flow.

At 15,000 rpm, the rotor wake velocity deficit and flow angle variations are on the order of 15% and 12 deg, with blade-to-blade wake variability of approximately 5% and 2 deg (Fig. 10). The stator vane response exhibits considerable variability over one complete rotor revolution, most notable in the unsteady lift. Also, the responses over the first and last (20th) blade pass periods are identical. This shows that blade-to-blade wake forcing function variability results in variability in the unsteady aerodynamic response of a downstream airfoil row, with the fundamental periodicity of both the forcing function and the resultant vane response one complete rotor revolution. Also, the shape and phase of the unsteady lift and moment waveforms closely resemble the unsteady static pressure measured 18.75% stator chord upstream of the vane. This suggests that part of the static pressure variation is indeed due to an acoustic interaction generated by the stator response to the rotor wakes.

At 18,000 rpm, the rotor wake velocity deficit is much more erratic, with the blade-to-blade wake differences of the same magnitude as the wakes themselves (Fig. 11). The flow angle variation

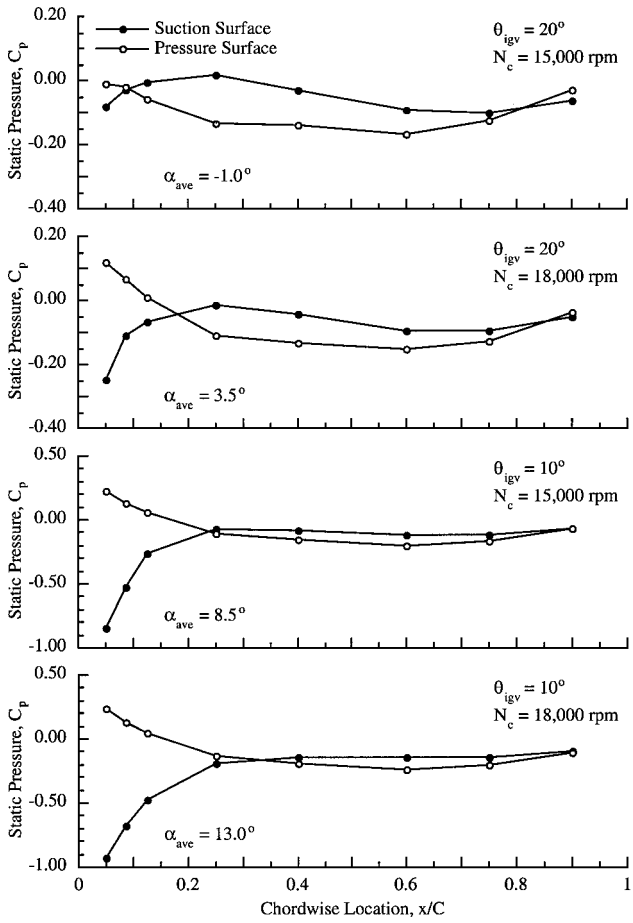

Fig. 9 Steady vane pressure distributions.

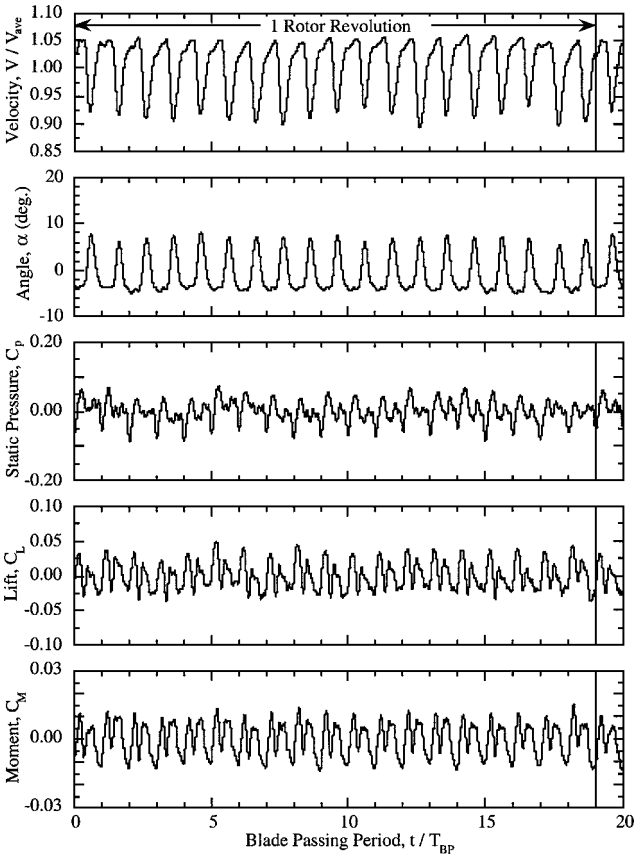

Fig. 10 Rotor wake and vane response, $\Delta S/S_{igv} = 0.00$, $\theta_{igv} = 20$ deg, and $N_c = 15{,}000$ rpm.

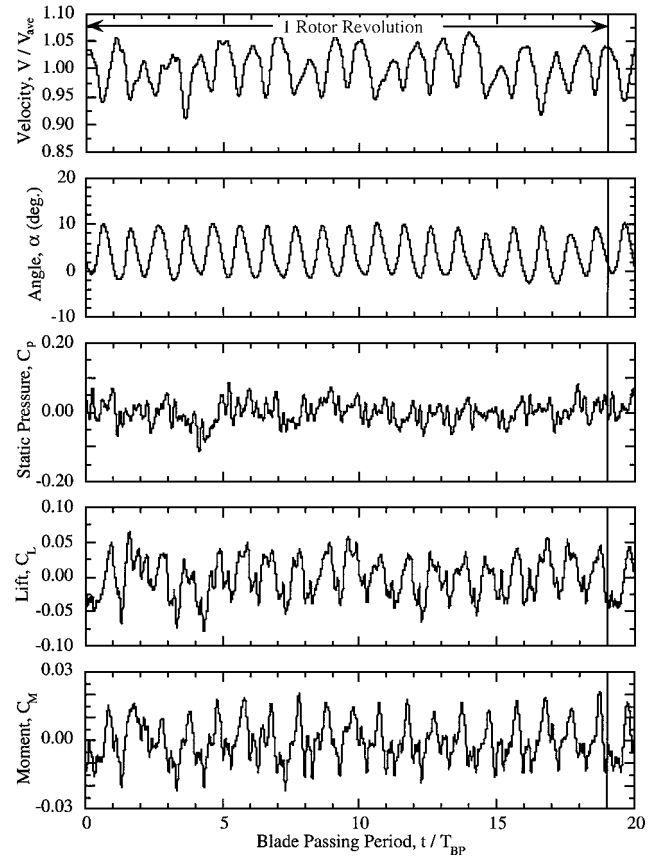

Fig. 11 Rotor wake and vane response, $\Delta S/S_{igv} = 0.00$, $\theta_{igv} = 20$ deg, and $N_c = 18{,}000$ rpm.

is much more uniform, but the profiles differ from blade to blade and are much wider than at 15,000 rpm. The stator response as well as the unsteady static pressure upstream of the vane also exhibit erratic behavior, with the variability much more pronounced than at 15,000 rpm. The erratic vane response is attributed to the erratic behavior of the forcing function, with the temporal periodicity over one complete rotor revolution. Again, the phase and shape of the unsteady static pressure upstream of the vane closely resemble the vane unsteady aerodynamic response.

Figures 12 and 13 show the rotor wake and resultant stator vane unsteady aerodynamic response at corrected speeds of 15,000 and 18,000 rpm for the 10-deg IGV stagger. The rogue wake is clearly evident at 15,000 rpm, with the velocity deficit nearly twice as large as the other wakes (Fig. 12). However, the rogue wake flow angle variation is the same as the other wakes. In fact, there is considerable variability in the velocity deficit but the flow angle is fairly uniform from blade to blade. There is also large variability in the vane response, again most pronounced for the unsteady lift. However, the stator does not respond to the rogue wake. This may be due in part to the signal conditioning, with the pressure transducer signals high-pass filtered at 500 Hz and the rogue wake having a passing frequency of 250 Hz. Also, the responses for the first and last (20th) blade pass periods differ slightly. This may be due to errors associated with the integration of the discrete pressure data and also the phase-lock averaging procedure, with 500 ensembles possibly insufficient to average out all random unsteadiness due to the high steady vane loading at this IGV stagger.

At 18,000 rpm, the wakes are wider and deeper than at 15,000 rpm (Fig. 13). However, the rotor exit flow is not as erratic as at 20-deg IGV stagger. This is because the rotor inlet relative Mach number is lower at the 10-deg IGV stagger due to less inlet preswirl. The rogue wake is also much less pronounced, with the rogue wake wider but the velocity deficit only a few percent larger than the other wakes. In contrast to the 15,000-rpm results, the blade-to-blade wake flow angle variability is large, on the order of 5 deg. From the flow angle

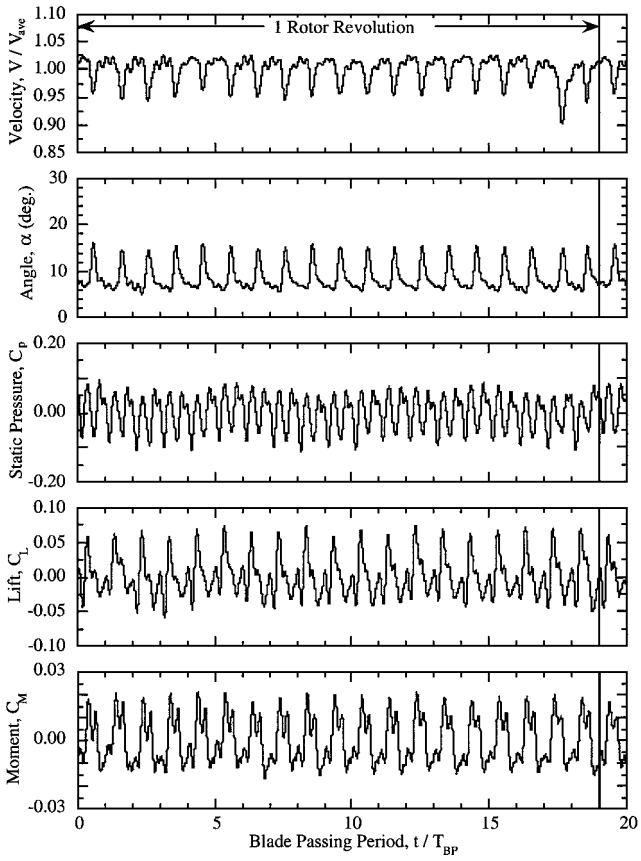

Fig. 12 Rotor wake and vane response, $\Delta S/S_{igv} = 0.00$, $\theta_{igv} = 10$ deg, and $N_c = 15{,}000$ rpm.

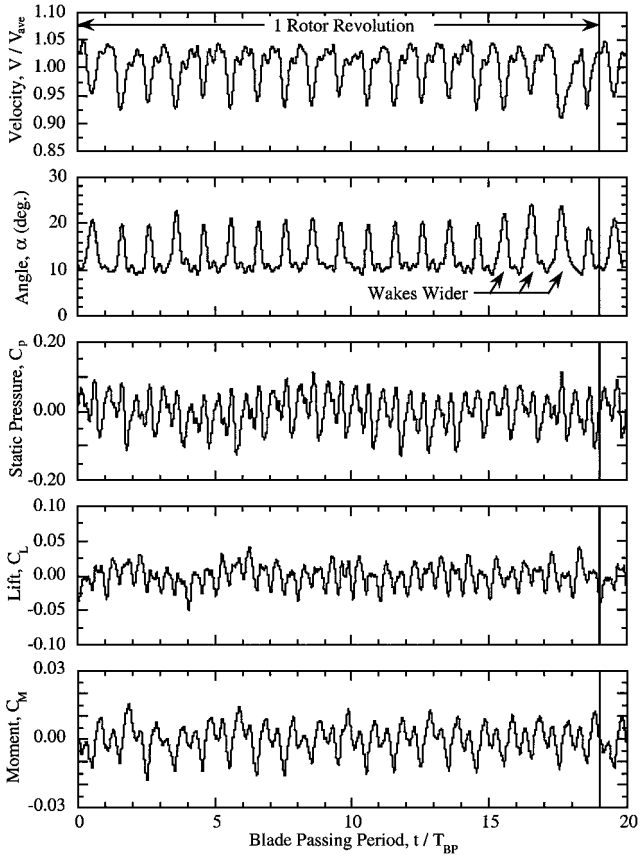

Fig. 13 Rotor wake and vane response, $\Delta S/S_{igv} = 0.00$, $\theta_{igv} = 10$ deg, and $N_c = 18{,}000$ rpm.

data, the wakes of the 15th, 16th, and 17th blades also appear much wider than those of the other blades. The variability of the unsteady lift and moment has also increased relative to the corresponding 15,000 rpm results, attributed to the larger blade-to-blade wake variability. Also, the responses for the first and last blade-pass periods are identical, again indicating that the fundamental periodicity is one complete rotor revolution.

Blade-to-Blade Wake and Response Variability

The blade-to-blade variability in the phase-lock-averaged rotor wake velocity deficit and the stator vane unsteady aerodynamic lift are also quantified with the IGV in the unclocked position. To obtain an integer number of data points per blade pass period, a new sampling rate was defined based on the measured rotor speed and the waveforms interpolated. This allows all 19 rotor wakes and the corresponding stator vane unsteady aerodynamic response to each wake to be compared directly to one another and the statistical variations to be determined, with the mean and standard deviation calculated by averaging corresponding points along each of the 19 wake and vane response blade pass periods.

Figures 14 and 15 present the 19 rotor wakes and the vane unsteady lift response to each wake for corrected speeds of 15,000 and 18,000 rpm at the 20-deg IGV stagger. The average or mean wake and vane response are denoted by the solid symbols, with the vertical bars representing ± 2 standard deviations ($\pm 2\sigma$) from the mean. The wake and corresponding vane response between the 17th and 18th blade pass periods are also shown by dashed lines because this was the time interval associated with the rogue wake.

At the design speed of 15,000 rpm, the largest variability is on the rotor wake suction side, with the pressure side of the wake and freestream region fairly uniform from blade to blade (Fig. 14). This variability is quite large, with the average velocity deficit approximately 13% and the 2σ bands about ± 5, ± 2, and $\pm 1\%$ of the time-average velocity for the suction side, pressure side, and freestream, respectively. For this clocking position, the rogue wake

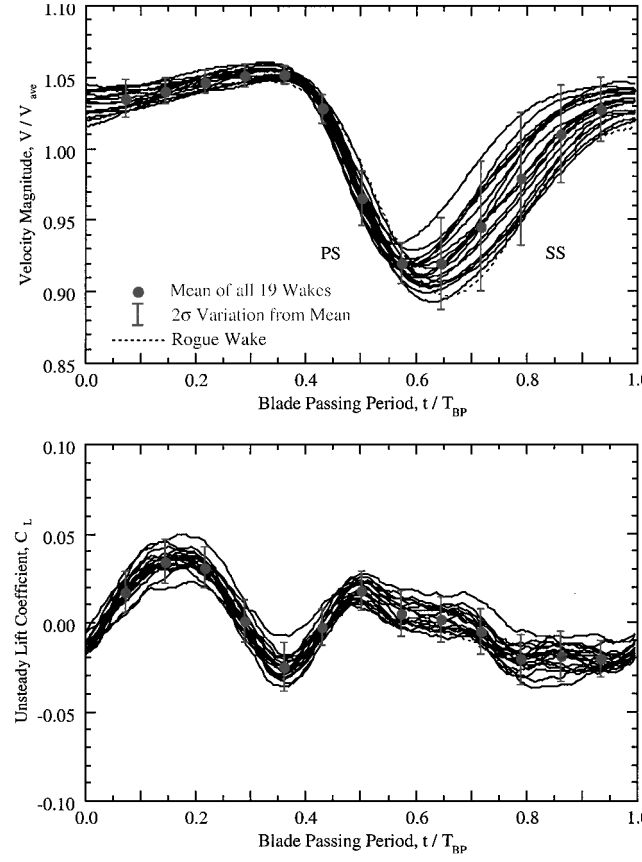

Fig. 14 Rotor wake and vane response variability, $\Delta S/S_{igv} = 0.00$, $\theta_{igv} = 20$ deg, and $N_c = 15{,}000$ rpm.

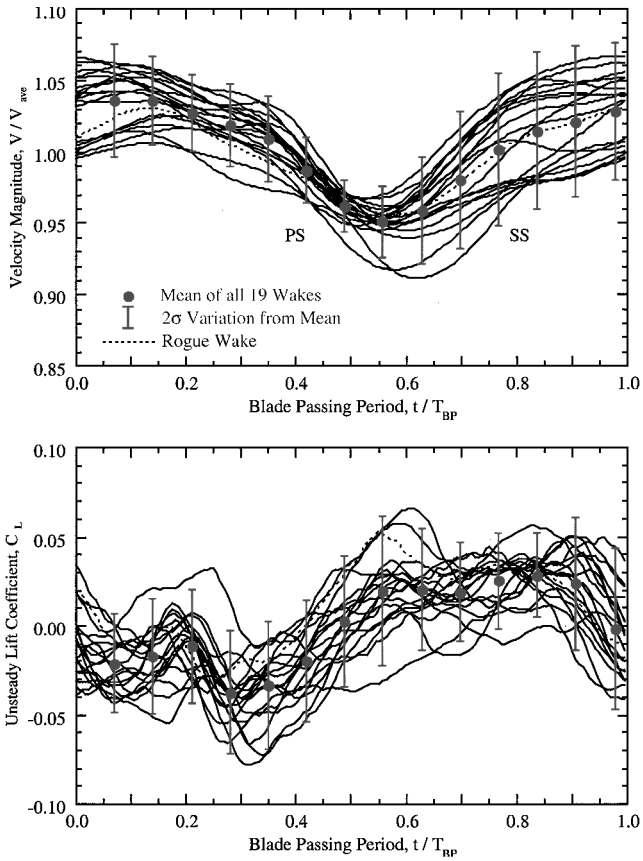

Fig. 15 Rotor wake and vane response variability, $\Delta S/S_{igv} = 0.00$, $\theta_{igv} = 20$ deg, and $N_c = 18{,}000$ rpm.

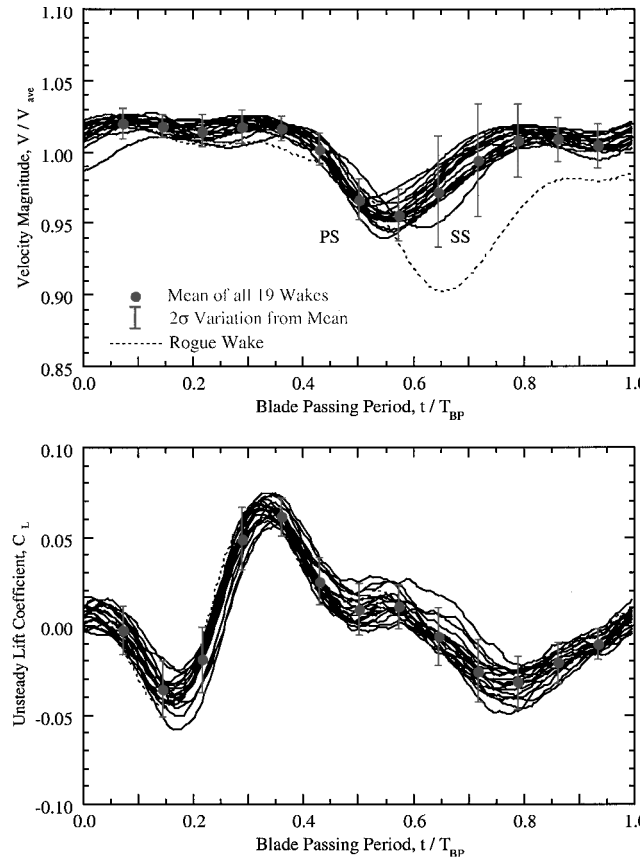

Fig. 16 Rotor wake and vane response variability, $\Delta S/S_{igv} = 0.00$, $\theta_{igv} = 10$ deg, and $N_c = 15{,}000$ rpm.

is not evident in the time traces. However, the wake that occurs between the 17th and 18th blade-pass periods exhibits the greatest variability from the mean. Thus, even in the unclocked position, the rotor blade that generates the rogue wake has a higher loss than the other blades. Also, the deeper wakes exhibit larger suction side semiwake widths, indicating that the rotor loss varies from blade to blade.

The vane response variability is even more marked, with the 2σ bands ± 0.015 nearly one-half the maximum of the average unsteady lift coefficient over one blade-pass period. Thus, small blade-to-blade differences in the wake forcing function lead to even greater variability in the resultant vane response. This indicates that the vane row does not respond to individual rotor blade wakes in a quasi-steady manner. Rather, the fundamental forcing function period is one rotor revolution.

At 18,000 rpm, there is considerable variability over the entire blade passage due to transonic flow effects (Fig. 15). This variability is very significant, with the 2σ bands for the freestream, pressure side, and suction side of the wake ± 4, ± 2, and $\pm 5\%$, respectively, with the average profile having a velocity deficit of 8%. The vane response variability is also much more marked than at 15,000 rpm, with the 2σ bands as large as ± 0.047, 160% of the maximum average unsteady lift over one blade-pass period. This large vane response variability is attributed to the increased blade-to-blade variability of the forcing function generated by off-design rotor operation, with this variability spread out over the entire 2σ band.

Figures 16 and 17 show the forcing function and vane response for the 10-deg IGV stagger. At 15,000 rpm, the blade-to-blade variability in the velocity deficit is fairly small except for the rogue wake (Fig. 17). Because the rogue wake has a velocity deficit almost twice as large as the mean for all 19 blades, it contributes substantially to the standard deviation. The 2σ bands for the freestream, pressure side, and suction side of the wake are near ± 1, ± 1.5, and $\pm 4\%$, respectively, and the average velocity deficit is near 6%. Also, the rogue wake is outside the 2σ band. Thus, it is not part of the Gaussian

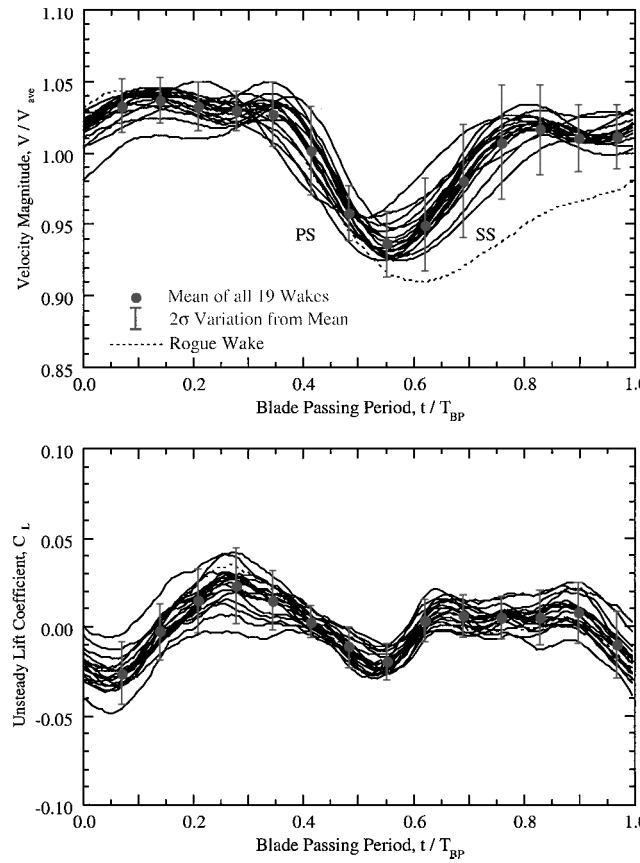

Fig. 17 Rotor wake and vane response variability, $\Delta S/S_{igv} = 0.00$, $\theta_{igv} = 10$ deg, and $N_c = 18{,}000$ rpm.

distribution describing the statistical variations of the wake. In fact, with the exclusion of the rogue wake, the variability associated with the suction side of the wake is on the order of $\pm 1\sigma$. The vane response variability for this configuration is smaller than that at 20-deg IGV stagger, but is still large, with the 2σ bands ± 0.021, nearly one-third of the maximum average unsteady lift occurring over one blade-pass period.

At 18,000 rpm, the rogue wake is much less pronounced but is still outside the 2σ band (Fig. 17). The variability is also smaller than at the 20-deg IGV stagger, with the average velocity deficit 9% and the 2σ bands ± 2, ± 3, and ± 4% for the freestream, pressure side, and suction side of the wake, respectively. The vane response variability is also very pronounced, with the 2σ bands as large as ± 0.021, nearly 90% of the maximum average unsteady lift.

Conclusions

High-speed rotor blade-to-blade wake variability and the resultant unsteady aerodynamic response of a downstream stator were experimentally investigated. The rotor wake changed markedly with IGV clocking, with both the wake character and the blade-to-blade variability affected. This was attributed to both wake chopping and transport of the IGV wake segments by the rotor and also the spinning acoustics modes generated by blade row coupling. At certain IGV clocking positions, the chopped IGV wake segments merged with the rotor wakes, thereby resulting in a very different forcing function to the downstream stator. A rogue wake was also generated by these multistage interactions, with the velocity deficit dependent on IGV clocking position and IGV stagger. The temporal periodicity of these multistage interactions was shown to be one complete rotor revolution due to the unequal number of blades and vanes. The time-variant waveforms corresponding to the unclocked and full-cycle IGV positions were also different, showing that the fundamental spatial periodicity of these interactions was over the entire annulus.

The variability in the unsteady aerodynamic response of the downstream stator over one complete rotor revolution was also investigated. Off-design rotor operation resulted in the largest blade-to-blade wake variability, which generated the largest variability in the vane response. The unsteady static pressure waveform upstream of the vane was markedly similar to the downstream vane unsteady response waveforms, indicating that the measured unsteady pressure field is due in part to the vane acoustic response to the rotor wakes.

The blade-to-blade rotor wake and resultant vane response variability were quantified. The wake width and depth exhibited considerable variability, most notably on the wake suction side. In fact, this variability can be of the same order as the average velocity deficit. Off-design rotor operation resulted in the largest variability, with the freestream region exhibiting almost as much variability as the wakes. The rogue wake velocity deficit was also greater than 2σ from the mean. The vane response variability was even more pronounced, with the unsteady lift variability ranging from 33 to 160% of the maximum average unsteady lift.

In summary, IGV clocking alters the rotor wake, demonstrating that it may be a viable passive stator vibration control technique. Multistage interactions also contributed to rotor blade-to-blade wake variability and to the generation of a rogue wake. Typically, data are acquired over only a few wake-passing periods. However, to accurately assess multistage interaction phenomena and to determine if rouge wakes exist, data corresponding to one complete rotor revolution must be acquired because this is the fundamental periodicity of these interactions. Also, computational fluid dynamics analyses must correctly account for unequal numbers of blades and vanes in the machine to predict accurately multistage interactions. Finally, small blade-to-blade wake differences lead to large variations in the downstream vane row unsteady aerodynamic response. Thus, models are needed to address aerodynamic mistuning effects on airfoil response, including rogue wake effects.

Acknowledgment

This research was sponsored by the Air Force Office of Scientific Research. This support is most gratefully acknowledged

References

[1] Smith, L. H., Jr., "Wake Dispersion in Turbomachines," *Journal of Basic Engineering*, Vol. 88, Sept. 1966, pp. 688–690.

[2] Kerrebrock, J. L., and Mikolajczak, A. A., "Intra-Stator Transport of Rotor Wakes and Its Effect on Compressor Performance," *Journal of Engineering for Power*, Vol. 92, Oct. 1970, pp. 359–368.

[3] Schmidt, D. P., and Okiishi, T. H., "Multistage Axial-Flow Turbomachine Wake Production, Transport, and Interaction," *AIAA Journal*, Vol. 15, No. 8, 1977, pp. 1138–1145.

[4] Sharma, O. P., Butler, T. L., Joslyn, H. D., and Dring, R. P., "Three-Dimensional Unsteady Flow in an Axial Flow Turbine," *Journal of Propulsion and Power*, Vol. 1, No. 1, 1985, pp. 29–38.

[5] Johnston, R. T., and Fleeter, S., "Airfoil Row Wake Interactions in a High Speed Axial Compressor," AIAA Paper 96-2821, 1996.

[6] Cherret, M. A., and Bryce, M. A., "Unsteady Viscous Flow in a High-Speed Core Compressor," *Journal of Turbomachinery*, Vol. 114, April 1992, pp. 287–294.

[7] Buffum, D. H., Capece, V. R., King, A. J., and El-Aini, Y. M., "Experimental Investigation of Unsteady Flows at Large Incidence Angles in a Linear Oscillating Cascade," AIAA Paper 96-2823, 1996.

[8] Johnston, R. T., and Fleeter, S., "Transonic Flow Effects on Fan Stage Interaction Generated Acoustic Modes," AIAA Paper 96-1678, 1996.

[9] Hall, K. C., and Silkowski, P. D., "The Influence of Neighboring Blade Rows on the Unsteady Aerodynamic Response of Cascades," American Society of Mechanical Engineers, ASME Paper 95-GT-35, 1995.